Available online at www.sciencedirect.com
ScienceDirect
Biomaterials 28 (2007) 1967–1977
Biomaterials
www.elsevier.com/locate/biomaterials

The effect of nanofiber alignment on the maturation of engineered meniscus constructs

Brendon M. Baker[a,b], Robert L. Mauck[a,b,*]

[a]McKay Orthopaedic Research Laboratory, Department of Orthopaedic Surgery, University of Pennsylvania, Philadelphia, PA 19104, USA
[b]Department of Bioengineering, University of Pennsylvania, Philadelphia, PA 19104, USA

Received 3 October 2006; accepted 1 January 2007
Available online 23 January 2007

Abstract

The fibrocartilaginous menisci are load-bearing tissues vital to the normal functioning of the knee. Removal of damaged regions of the meniscus subsequent to injury impairs knee function and predisposes patients to osteoarthritis. In this study, we employed biodegradable nanofibrous scaffolds for the tissue engineering of the meniscus. Non-aligned (NA) or fiber-aligned (AL) nanofibrous scaffolds were seeded with meniscal fibrochondrocytes (MFCs) or mesenchymal stem cells (MSCs) to test the hypothesis that fiber-alignment would augment matrix content and organization, resulting in improved mechanical properties. Additionally, we proposed that MSCs could serve as an alternative to MFCs. With time in culture, MSC- and MFC-seeded NA and AL constructs increased in cellularity and extracellular matrix (ECM) content. Counter our initial hypothesis, NA and AL constructs contained comparable amounts of ECM, although a significantly larger increase in mechanical properties was observed for AL compared to NA constructs seeded with either cell type. Cell-seeded NA constructs increased in modulus by ~1 MPa over 10 weeks while cell-seeded AL construct increased by >7 MPa. Additionally, MSC-constructs yielded greater amounts of ECM and demonstrated comparable increases in mechanical properties, thereby confirming the utility of MSCs for meniscus tissue engineering. These results demonstrate that cell-seeded fiber-aligned nanofibrous scaffolds may serve as an instructive micro-pattern for directed tissue growth, reconstituting both the form and function of the native tissue.

Keywords: Tissue engineering; Mechanical properties; Electrospinning; Anisotropy; Fibrochondrocytes; Mesenchymal stem cells

1. Introduction

The menisci are a pair of fibrocartilaginous wedges that play a central role in knee mechanics, increasing congruency and joint stability [1,2]. With normal use, forces of several times body weight arise within the knee, with the menisci transmitting 50–100% of this load [3,4] through its dense network of circumferentially aligned (AL) collagen [5–8]. This ordered architecture engenders very high tensile properties in the fiber direction (50–300 MPa) [6,7,9]. Collagens make up 85–95% of the tissue [10,11], while proteoglycans (PGs) comprise 2–3% of the dry weight, are concentrated in the cartilage-like inner regions [12,13], and contribute to the compressive properties of the tissue. This extracellular matrix (ECM) is generated and maintained by meniscal fibrochondrocytes (MFCs), a heterogeneous cell population sparsely distributed throughout the tissue [10,12,14].

While the meniscus functions well with normal use, failures may occur as a result of traumatic injury or degenerative processes [15,16]. Repaired tears in the vascular periphery heal well, while those in the avascular inner region fail to do so, and thus damaged elements are commonly resected via partial meniscectomy. Removal of tissue results in higher cartilage contact stresses which may predispose patients to osteoarthritic (OA) progression.

*Corresponding author. McKay Orthopaedic Research Laboratory, Department of Orthopaedic Surgery, University of Pennsylvania, 424G Stemmler Hall, 36th Street and Hamilton Walk, Philadelphia, PA 19104. Tel.: +215 898 3294; fax: +215 573 2133.
E-mail address: lemauck@mail.med.upenn.edu (R.L. Mauck).

0142-9612/$ - see front matter © 2007 Elsevier Ltd. All rights reserved.
doi:10.1016/j.biomaterials.2007.01.004

Replacing damaged regions of the meniscus with a living, biodegradable, mechanically competent construct may restore function and protect against further deleterious changes in the joint.

To this end, a number of tissue engineering strategies for restoring the meniscus have been developed. These strategies include the delivery of cells to the defect site, including chondrocytes, MFCs, and mesenchymal stem cells (MSCs) [17–19]. Additionally, direct replacement has been performed using both natural and synthetic scaffolds, including collagen-based grafts and macroporous polymeric meshes [20–22]. These studies suggest that cell- and scaffold-based interventions hold promise for effective meniscus repair.

To further this area of inquiry, we focus on the generation of engineered meniscus constructs using nanofibrous biodegradable scaffolds formed via electrospinning. In this process, non-woven fibrous meshes are generated with fiber diameters on the order of hundreds of nanometers [23,24]. These nanofibrous scaffolds can be produced from a range of polymers and biopolymers [25–29], with composition dictating the as-formed mechanical properties of the mesh and its degradation rate. Numerous cell types attach to, differentiate on, and infiltrate these scaffolds, including MFCs and MSCs [30–32].

As described above, the fiber architecture and alignment of the meniscus endows the tissue with its unique functional properties. As such, this architecture must be one of the first considerations when engineering replacement constructs. To address this issue, nanofibrous meshes with controlled fiber alignment were produced by directing fiber deposition onto a rotating shaft [33,34], with the degree of alignment controlled by the target rotation speed. This controllable architecture in turn dictates the anisotropic mechanical properties of the scaffold [25,30,35,36]. In this study, we hypothesize that, when seeded with cells, AL scaffolds will serve as a 3D micro-pattern for directing neo-tissue formation, resulting in a mature construct with enhanced matrix content, organization, and mechanical properties compared to non-aligned (NA) scaffolds similarly maintained. Further, we test the hypothesis that MSCs may serve as a viable alternative to MFCs. To evaluate these hypotheses, MSCs and MFCs were seeded on both NA and AL nanofibrous scaffolds and cultured over a 10-week period in a chemically defined chondrogenic medium. We evaluated initial cell–scaffold interactions and long-term accumulation and distribution of ECM and the resulting change in mechanical properties.

2. Materials and methods

2.1. Nanofibrous scaffold production

Poly(ε-caprolactone) (PCL) nanofiber meshes were produced via electrospinning as described in [32]. Briefly, a 14.3% w/v solution of PCL (Sigma, 80 kD) was prepared in a 1:1 solution of tetrahydrofuran and *N*,*N*-dimethylformamide (Fisher Chemical, Fairlawn, NJ) with continuous agitation over 72 h. A total of 10 ml of the polymer solution was gravity fed from a vertically oriented 10 ml syringe fitted with a stainless-steel 18-G blunt needle, the end of which was positioned 20 cm above a grounded collecting surface. For NA scaffolds, the collecting surface consisted of a stationary copper plate covered with aluminum foil. To produce AL scaffolds, the copper plate was replaced with a mandrel (1″ diameter, 8″ length) rotating at ~7500 rpm, corresponding to a linear velocity of ~10 m/s [37]. A power supply (Gamma High Voltage Research Inc., Ormond Beach, FL) was used to apply a 13 kV potential difference between the needle and the collecting surface. Nanofibers were collected for 12–16 h, resulting in a fiber mat ranging in thickness from 0.9 to 1.3 mm. NA and AL scaffolds used in this study were of similar thicknesses and distribution (NA: 1.14 mm, AL: 1.11 mm, $p > 0.487$).

2.2. Cell isolation and expansion

MFCs were isolated from the lateral and medial menisci of 3–6-month-old calves. MSCs were isolated from the tibial trabecular bone marrow of the same animals. For each replicate study, cells isolated from a minimum of three donors were pooled. For MFC isolation, menisci were diced into 1–2 mm^3 pieces and placed in tissue culture dishes with basal medium (DMEM containing 1× PSF (100 units/ml penicillin, 100 μg/ml streptomycin, 0.25 μg/ml fungizone) and 10% fetal bovine serum (FBS)). MFCs emerged from these pieces over a 1–2-week period and were sub-cultured at a 1:3 ratio through passage 2 as in [38]. MSCs were harvested from the tibial trabecular bone marrow of the same donors as in [39]. Briefly, the proximal end of the tibia was sectioned and trabecular marrow freed into DMEM supplemented with 300 units/mL heparin. After centrifugation for 5 min at 500*g*, pelleted matter was resuspended in basal medium and plated in 150 mm tissue culture dishes. Adherent cells formed numerous colonies through the first week, and were subsequently expanded through passage 2 at a ratio of 1:3 as above.

2.3. Scaffold seeding and culture

To produce cell-seeded constructs, individual scaffolds were excised as strips from nanofibrous sheets at 25 mm length by 5 mm width. For AL sheets, the long axis of the construct corresponded to the prevailing fiber direction. Strips were disinfected and rehydrated with decreasing concentrations of ethanol (100%, 70%, 50%, 30%; 30 min per step). For acellular degradation studies, constructs were incubated in phosphate-buffered saline (PBS) at 37 °C. For cell-seeding studies, the rehydration step was concluded by incubation in 20 μg/mL fibronectin in PBS for 12 h followed by two 5 min washes in PBS. To seed scaffolds, 50 μl aliquots containing 2.5×10^5 cells (MSCs or MFCs) were loaded onto each scaffold four times (twice per side) at 30 min intervals. After allowing an additional 2 h for cell attachment, seeded constructs were cultured in 3 mL of chemically defined medium (high glucose DMEM with 1× PSF, 0.1 μM dexamethasone, 50 μg/mL ascorbate 2-phosphate, 40 μg/mL L-proline, 100 μg/mL sodium pyruvate, 1× ITS+ (6.25 μg/ml insulin, 6.25 μg/ml transferrin, 6.25 ng/ml selenous acid, 1.25 mg/ml bovine serum albumin, and 5.35 μg/ml linoleic acid) with 10 ng/mL TGF-β3) in non-tissue culture treated 6-well plates. This chemically defined media formulation was used as it has previously been shown to both induce chondrogenesis of MSCs as well as promote deposition of fibrocartilaginous ECM by MFCs in pellet culture [38]. Media (and PBS) were changed twice weekly over a 10-week period.

2.4. Visualization of cell–scaffold interactions

NA and AL scaffolds seeded with MSCs were examined with the Live/Dead kit (Molecular Probes, Eugene, OR) after 24 h of culture to visualize cell morphology. Images of calcein AM-stained MSCs on AL and NA scaffolds were acquired with an inverted fluorescent microscope (Axiovert 200, Carl Zeiss MicroImaging Inc., Thornwood, NY) at a magnification of

Table 1
Change in measured parameters (compared to day 1) for two replicate studies of MFC- and MSC-laden AL and NA nanofibrous scaffolds over 70 days in free swelling culture

	Study 1[a]				Study 2			
Cell type	MFC		MSC		MFC		MSC	
Scaffold alignment	NA	AL	NA	AL	NA	AL	NA	AL
ΔMass (mg)	3.3	2.8	2.5	2.5	5.6	5.1	8.8	6.5
ΔDNA (ng)	8.9	9.2	5.3	7.3	11.8	13.0	9.6	10.2
ΔGAG (μg)	104	161	151	303	165	203	325	405
ΔCollagen (μg)	119	173	162	213	124	133	139	206
ΔStiffness (N/mm)	0.4	4.2	0.7	4.5	0.1	5.6	1.0	6.8
ΔModulus (MPa)	1.0	7.6	1.4	7.2	−0.4	4.4	1.3	7.2

[a]Data from Study 1 are plotted in this manuscript.

20×. Additional samples were fixed in phosphate-buffered 4% paraformaldehyde for imaging with scanning electron microscopy (SEM). These specimens were dehydrated in ethanol (four steps, 30–100%, 60 min per step) with terminal dehydration in hexamethyldisilane under vacuum [40]. After AuPd sputter coating, SEM was used to image both acellular and cell-seeded scaffolds (JEOL 6400, Penn Regional Nanotechnology Facility).

2.5. Mechanical testing

Uniaxial tensile testing was performed with an Instron 5848 Microtester equipped with serrated vise grips and a 50 N load cell (Instron, Canton, MA). A 0.5 N preload was applied for 180 s to ensure proper seating of the sample. An externally mounted digital camera was used to obtain sample thickness and width from front and side views of the preloaded sample. After noting gauge length with a digital caliper, samples were preconditioned with 10 cycles of 0.5% of gauge length at 0.1 Hz and subsequently extended to failure at 0.1% of gauge length per second. Construct stiffness was determined from the linear region of the force–elongation curve. Construct modulus was determined from these data based on the sample geometry and measured gauge length.

2.6. Biochemical content

After testing, samples were stored at −80 °C until processing for biochemical composition. Samples were lyophilized in a Freezone 4.5 Freeze Dry System (LabConco, Kansas City, MO) for 24 h and weighted to determine dry weight. After papain digest as in [39], samples were processed for DNA, sulfated glycosaminoglycan (s-GAG), and collagen content using the Picogreen double-stranded DNA (dsDNA) (Molecular Probes, Eugene, OR), DMMB dye-binding [41], and orthohydroxyproline [42] assays, respectively. These data are reported as mass of ECM element (s-GAG or collagen) per construct and as ECM content normalized to DNA content.

2.7. Histological analysis

At each time point, samples were fixed overnight at 4 °C in 4% phosphate-buffered paraformaldehyde, washed in PBS, and frozen in Optimal Cutting Temperature compound (OCT, Sakura Finetek USA Inc., Torrance, CA). Cross-sections (spanning the depth and width of the scaffold) were cut to 8 μm with a Cryostat (Microm HM500, MICROM International GmbH, Waldorf, Germany). Sections were rehydrated and stained with haematoxylin and eosin (H&E), Alcian blue (AB, pH 1.0), or Picrosirius red (PSR) for cells, PGs, or collagens, respectively. On separate samples at the terminal time point (day 70), serial 8 μm sections through the depth were removed *en face* (in the length–width plane of the scaffold). *En face* sections taken deep to the scaffold surface were stained with PSR to enhance birefringence and imaged using a polarizing light microscopy system (DMLP, Leica Microsystems, Germany) to assess collagen organization. Images were acquired at a magnification of 5× for cross-sections and 10× for *en face* sections with a color CCD digital camera.

2.8. Statistical analysis

Analysis of variance (ANOVA) was carried out with SYSTAT (v10.2, Point Richmond, CA) with Fisher's LSD *post hoc* tests used to make pairwise comparisons between groups, with significance set at $p \leqslant 0.05$. For both cellular and acellular (degradation) studies, two replicate studies were carried out with distinct donors and scaffold productions, with $\geqslant 5$ samples analyzed per assay per replicate. Data from cellular studies are presented as mean ± standard deviation (SD) for a single replicate study, with terminal data from both replicates shown in Table 1.

3. Results

3.1. Scaffold characterization and cellular interactions

As we have previously reported [36,37], NA nanofibrous scaffolds can be generated with deposition onto a stationary, grounded collecting plate (Fig. 1A), while an organized AL array of these same fibers may be generated by replacing the plate with a rotating mandrel (Fig. 1B). In this study, orientation and shape of cells (MFCs or MSCs) were dictated by the scaffold architecture. For example, after 1 day in culture, MSCs viewed via SEM (Fig. 1C and D) and by vital staining (Fig. 1E and F) appeared polygonal on NA scaffolds while those on AL scaffolds took on a polarized morphology with their long axis oriented in the prevailing fiber direction. When acellular NA and AL scaffolds were incubated for 70 days in PBS, no change in mechanical properties was observed (data not shown, NA: $p > 0.83$, AL, $p > 0.09$, $n = 5$–10 per time point).

3.2. Biochemical content of cell-laden scaffolds

To assess long-term maturation of constructs, cell-seeded scaffolds were cultured for 10 weeks in a chemically defined medium in two replicate studies. Data from one representative study is shown, with the change in measured

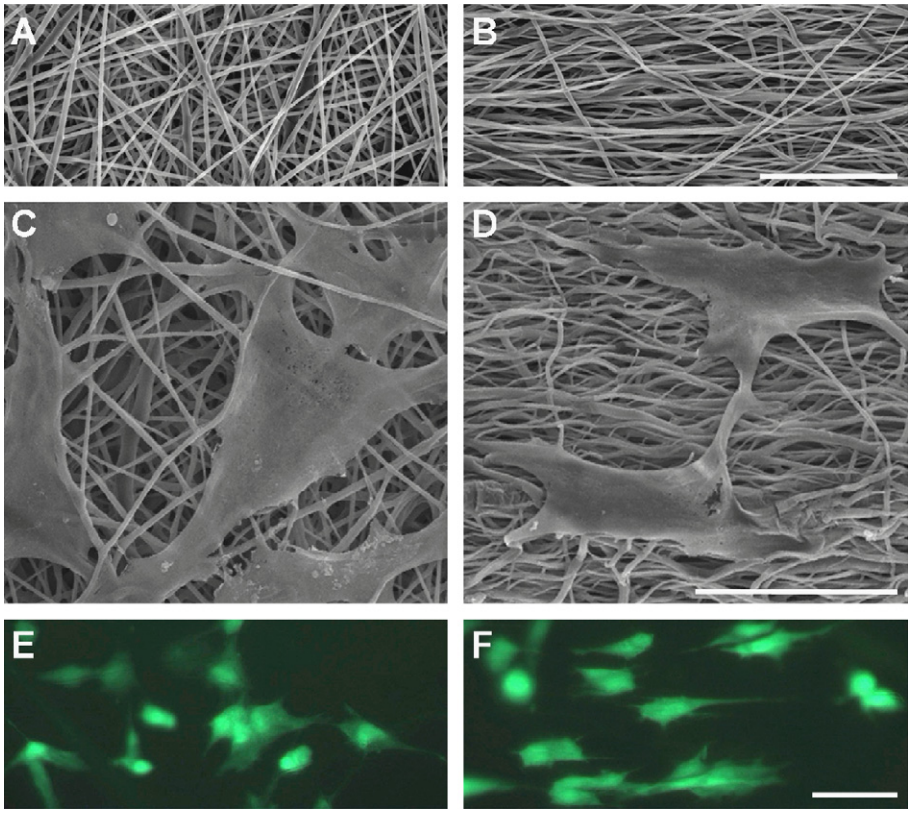

Fig. 1. Biodegradable scaffolds with sub-micron fiber diameters may be formed with randomly oriented fibers or with a distinct fiber alignment. Fibrous architecture dictates initial cell–scaffold interactions, including shape and polarity. SEM images of acellular (A) non-aligned (NA) and (B) aligned (AL) scaffolds. SEM and fluorescent images of MSCs on NA (C, E) and AL (D, F) scaffolds after one day of culture. Scale bar: 50 μm.

parameters over the time course for each replicate provided in Table 1.

With time, both MSC- and MFC-laden constructs increased in mass (Fig. 2A). Irrespective of scaffold architecture, an ~3 mg increase in mass was observed for both cell types over 10 weeks ($p<0.05$). Additionally, constructs thickened with time (data not shown, $p<0.005$), increasing by ~40% by day 70. Cell number, as measured by DNA content, was dependent on time in culture ($p<0.001$), scaffold alignment ($p<0.001$), and cell type ($p<0.001$). Notably, DNA content increased in both MSC and MFC-seeded constructs up to day 42, after which levels plateaued (Fig. 2B). At the final time point, MSC-seeded constructs contained fewer cells than MFC-seeded constructs (AL: $p<0.05$, NA: $p<0.001$).

ECM content also increased in constructs in a time-dependent manner. s-GAG content increased in all groups by day 42 (Fig. 3A, $p<0.001$). For this replicate study, all groups, with the exception of NA-MSC, continued to increase in s-GAG content through day 70. Overall, the total s-GAG per construct was highly dependent on time in culture ($p<0.001$) and cell type ($p<0.001$). While there were differences in s-GAG content observed between AL and NA scaffolds at certain time points (particularly at day 70), neither architecture resulted in consistently higher s-GAG content at every time point. Similar trends were seen after normalizing s-GAG to DNA content. By day 42, MSCs seeded on both NA and AL scaffolds produced higher amounts of s-GAG (and s-GAG/DNA) than their MFC counterparts (Fig. 3A and B, $p<0.001$).

Total collagen per construct was dependent on time ($p<0.001$), cell type ($p<0.001$), and alignment ($p<0.001$, Fig. 4A). Collagen was not detectable in day 1 samples. By day 14, collagen was detected in all groups and significant increases were observed between days 14 and 42 ($p<0.001$), as well as from day 42 to 70 ($p<0.001$). As with s-GAG content, MSC-seeded constructs contained higher collagen than MFC-seeded constructs, irrespective of underlying architecture, from day 42 forward ($p<0.001$). Within a cell type, no difference was observed between AL and NA constructs at days 14 (MSC: $p>0.16$, MFC: $p>0.23$) and 42 (MSC: $p>0.20$, MFC: $p>0.57$). On day 70, modest increases were seen in the collagen content of AL compared to NA constructs for both cell types ($p<0.001$). These findings suggest that scaffold alignment has less effect on collagen production than time in culture or cell type. For collagen data normalized to DNA content (Fig. 4B), cell type had a strong influence ($p<0.001$) while scaffold architecture had no effect ($p>0.75$), even on day 70. Irrespective of architecture, MSC-laden constructs

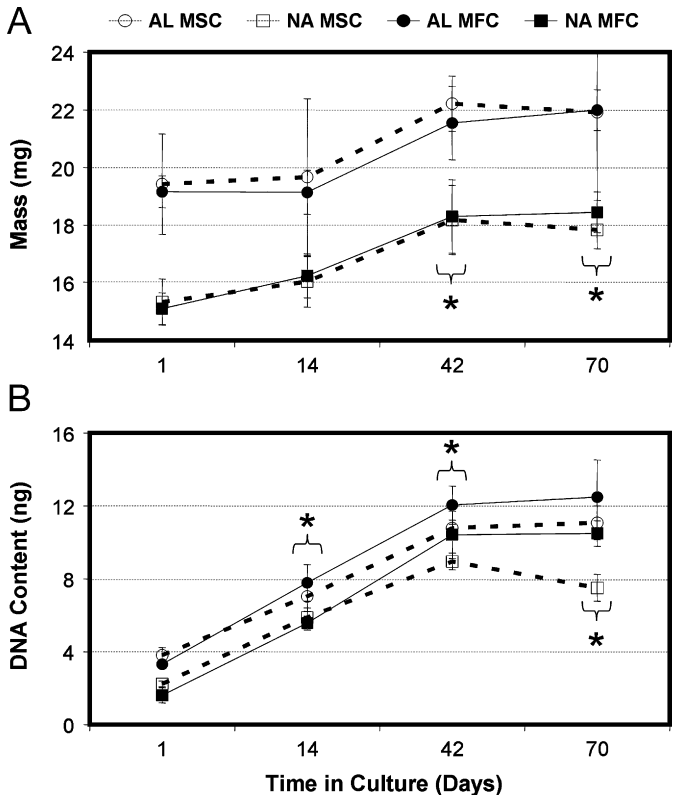

Fig. 2. Cell-seeded constructs increase in mass and DNA content with time in culture. Construct mass (A) and DNA content (B) of MFC- and MSC-laden AL and NA nanofibrous scaffolds. *Indicates $p<0.05$ vs. day 1 within group for construct mass (bracket indicates all groups at time point); *Indicates $p<0.001$ vs. day 1 within group for DNA content, $n=5$ per group per time point.

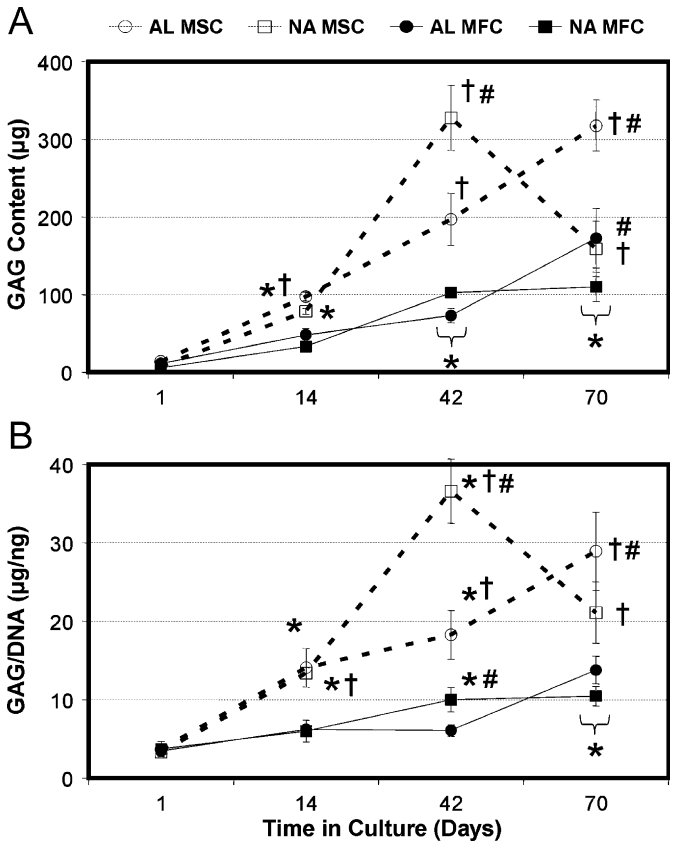

Fig. 3. MFCs and MSCs deposit a proteoglycan-rich matrix on NA and AL scaffolds with time in culture. Total s-GAG content per scaffold (A) and s-GAG content normalized to DNA (B) of MFC- and MSC-laden AL and NA nanofibrous scaffolds with time in culture. *Indicates $p<0.001$ vs. day 1 within group; #Indicates $p<0.001$ vs. NA within same cell type at same time point; †Indicates $p<0.001$ vs. MFC group of same alignment at same time point, $n=5$ per group per time point.

contained more collagen per cell than MFC-laden constructs on days 14 ($p<0.05$), 42 ($p<0.001$), and 70 ($p<0.001$).

3.3. Histologic appearance of cell-laden scaffolds

Cell localization and regional distribution of matrix deposition were assessed by staining of construct cross sections with time in culture (1–70 days), cell type (MFC and MSC), and scaffold architecture (NA and AL). No striking differences were observed between NA and AL scaffolds, and so the time course of cell infiltration is shown only for AL scaffolds for each cell type. H&E staining revealed a time-dependent progression of cellular infiltration (Fig. 5). On day 1, a sparse cell population was observed on the periphery (data not shown) that by day 14 completely covered the construct and had penetrated through the outer 100–200 µm (Fig. 5A and B). By day 42, constructs were covered with a multi-layer sheath of cells (Fig. 5C and D), with some cells penetrating to depths of ~300 µm from each edge. By day 70, MFCs and MSCs colonized the entire scaffold thickness, though they remained less dense at the center compared to the edge (Fig. 5E and F). A similar time course and final degree of colonization was observed for NA scaffolds seeded with both cell types (Fig. 5G and H).

Over the same time course, PG staining became more intense for both cell types, regardless of scaffold alignment (data not shown). At early times, PG was most concentrated at the scaffold periphery (coincident with cells), though a deep and homogenous distribution was seen by day 70 for both MSC- and MFC-seeded constructs (Fig. 6A and B). PG staining was generally greater for MSC- than for MFC-seeded constructs. Compared to PG staining, collagen was more heavily concentrated at the scaffold boundary (Fig. 6C and D). By day 70, the outer ~300 µm of each side of the scaffold showed similar staining intensity. Differences between MSC- and MFC-seeded constructs were less prominent than for PG staining. Alignment of collagenous matrix in day 70 *en face* sections taken ~200 µm deep to the construct surface showed a marked difference in organization in AL compared to NA constructs for both cell types (Fig. 7). Specifically, while abundant PSR staining was observed in *en face* sections for both NA and AL scaffolds, more intense birefringence (orange in polarized images) corresponded to AL collagen deposition only in AL constructs.

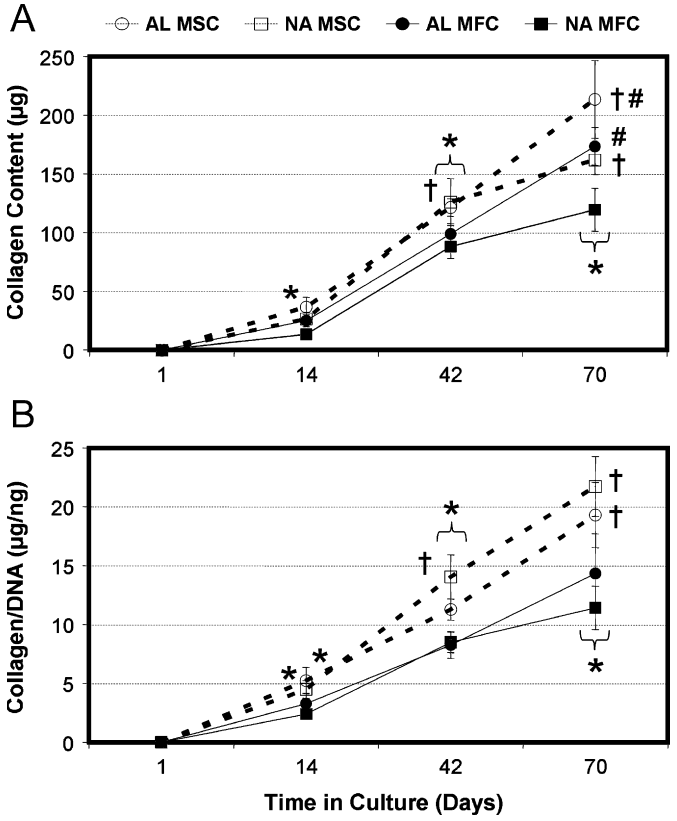

Fig. 4. MFCs and MSCs deposit a collagen-rich matrix on NA and AL scaffolds with time in culture. Total collagen content per scaffold (A) and collagen content normalized to DNA (B) of MFC- and MSC-laden AL and NA nanofibrous scaffolds with time in culture. *Indicates $p<0.001$ vs. day 1 within group; #Indicates $p<0.001$ vs. NA within same cell type at same time point; †Indicates $p<0.001$ vs. MFC group of same alignment at same time point, $n=5$ per group per time point.

3.4. Tensile mechanical properties of cell-laden scaffolds

Tensile testing was carried out to determine the contribution of newly formed matrix to the load-bearing capacity of constructs with time in culture (stiffness, Fig. 8A; modulus, Fig. 8B). At the outset of culture (day 1), stiffness and modulus of AL scaffolds were ~3-fold higher than NA scaffolds ($p<0.001$). For cell-seeded scaffolds, both time in culture ($p<0.001$) and scaffold alignment ($p<0.001$) were determining factors in the mechanical properties of each construct, while cell type was not ($p>0.344$). NA constructs, regardless of cell type, showed a nominal increase in modulus. For example MFC-seeded NA constructs increased from 4.0 MPa on day 1 to 5.0 MPa on day 70, a 25% increase. Similarly, the stiffness of these constructs increased from 1.5 to 1.8 N/mm. In contrast, MFC-laden AL constructs increased in modulus over the same time course, from 12.1 to 19.7 MPa, a 63% increase ($p<0.001$). Likewise, these constructs nearly doubled in stiffness from 4.5 N/mm on day 1 to 8.7 N/mm on day 70. Notably, these increases in mechanical properties were directed by the AL scaffold architecture and not cell type, as MSCs performed similarly to MFCs in both replicate studies (Table 1).

4. Discussion

The mechanical function of the meniscus is dependent on its unique fiber-aligned collagen architecture. When damage occurs, this architecture is interrupted and the ability of the meniscus to transmit load is compromised [1]. In this study, we address the repair of such defects with the fabrication and maturation of meniscus constructs using nanofibrous scaffolds whose architecture and anisotropy mimic that of the native tissue. We evaluated NA and AL nanofibrous meshes (Fig. 1) formed from PCL, a slow degrading polyester. As we have previously reported [36], deposition of PCL nanofibers onto a rotating mandrel results in scaffolds with significant anisotropy, such that AL scaffolds tested in the fiber direction were three times stiffer than NA scaffolds at the outset of the study (Fig. 8). Further, nanofibrous meshes formed from PCL maintain their organization and fiber diameter for long time periods in physiologic conditions, offering a stable micro-pattern for directed matrix deposition [27].

When seeded with MFCs or MSCs, the underlying architecture of the nanofibrous scaffolds directed cellular morphology. The aligned cellular arrays produced in this study are similar to those observed when cells are exposed to micro-contact printed strips [43,44] and topographic channels [45] in monolayer cultures. During culture in a chemically defined medium, cells divided and occupied the entirety of the scaffold, and deposited a fibrocartilaginous matrix similar in composition to the native tissue. This ECM contributed to time-dependent increases in the mechanical properties of the construct. Most strikingly, these increases depended primarily on underlying scaffold architecture—both MSC- and MFC-seeded NA scaffolds increased by ~1 MPa, while these same cells increased AL scaffold properties by >7 MPa. Interestingly, while marked increases in mechanical properties only occurred with AL scaffolds (Fig. 8), both cell types on NA and AL scaffolds resulted in similar cell content and degree of infiltration as well as comparable bulk quantities of ECM (Figs. 3 and 4). This finding is counter to that previously observed on AL polyurethane nanofibers after 1 week of culture, where AL scaffolds increased collagen deposition by ligament fibroblasts compared to NA scaffolds [46]. In aligned monolayer cultures, linear arrays of fibroblasts organize their collagen deposition with respect to the underlying surface topography [45]. Preliminary analysis of collagen organization suggests a similar mechanism at work in AL scaffolds, with pronounced collagen alignment observed under polarized light (Fig. 7). These findings suggest that AL scaffolds serve as a 3D micro-pattern for directing both the short- and long-term organization of cells and newly deposited ECM, and that this organization, rather than the amount of matrix produced, dictates the functional maturation of these meniscal constructs.

At the outset of this study, we hypothesized that, given their ability to undergo mixed fibrous/cartilaginous differentiation, MSCs may serve as a useful alternative to MFCs

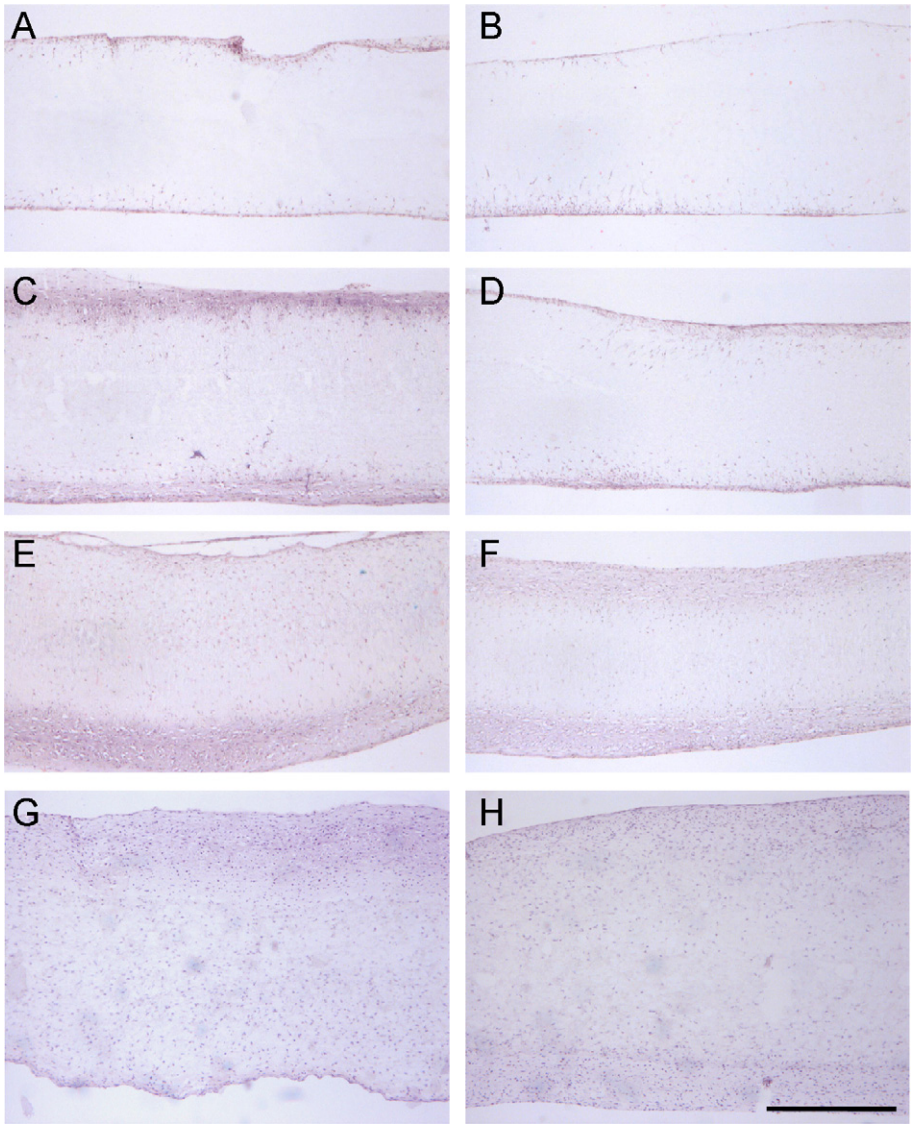

Fig. 5. MFCs and MSCs infiltrate nanofibrous scaffolds in a time-dependent fashion, with full colonization occurring between days 42 and 70. H&E staining of cross sections of MSC- (A, C, E) and MFC- (B, D, F) laden AL scaffolds on days 14 (A, B), 42 (C, D), and 70 (E, F). NA scaffolds seeded with MSCs (G) and MFCs (H) on day 70 are shown for comparison. Scale bar: 500 μm.

for the production of meniscus constructs. The clinical need for an alternative to MFCs arises from the scarcity of healthy autologous cells, and the fact that invasive surgical procedures are required for their isolation. MSCs may be suitable for this application, as they are readily available from bone marrow [47], and can be isolated from aged donors without significant loss in fibrocartilaginous potential [48]. The results of this study show that MSC-laden constructs produce higher levels of collagen and PG than MFC-laden scaffolds similarly maintained. Importantly, the MSC-deposited matrix is functional, leading to equivalent gains in the mechanical properties of constructs seeded with either cell type. It should be noted that the analyses carried out in this study were solely bulk measures of PG and collagen accumulation. Quantitative assessment of meniscus-specific matrix components, such as collagen types as well as expression and distribution of decorin, versican, and biglycan [14,49], may shed further light on similarities and differences between MFCs and MSCs, as well as the macromolecular underpinnings of the improvement of functional mechanical properties seen in AL compared to NA scaffolds in this study. Nevertheless, these findings do demonstrate the potential of MSCs to colonize and produce mechanically functional ECM in AL nanofibrous scaffolds in a manner similar to healthy primary MFCs, indicating their potential for meniscus tissue engineering applications.

While the results of this study are promising and repeatable (Table 1), several issues remain to be optimized in the production of a functional construct for meniscus repair. First, the mechanical properties of cell-seeded AL scaffolds approach only ~20 MPa, a value ~1/10th [9] to

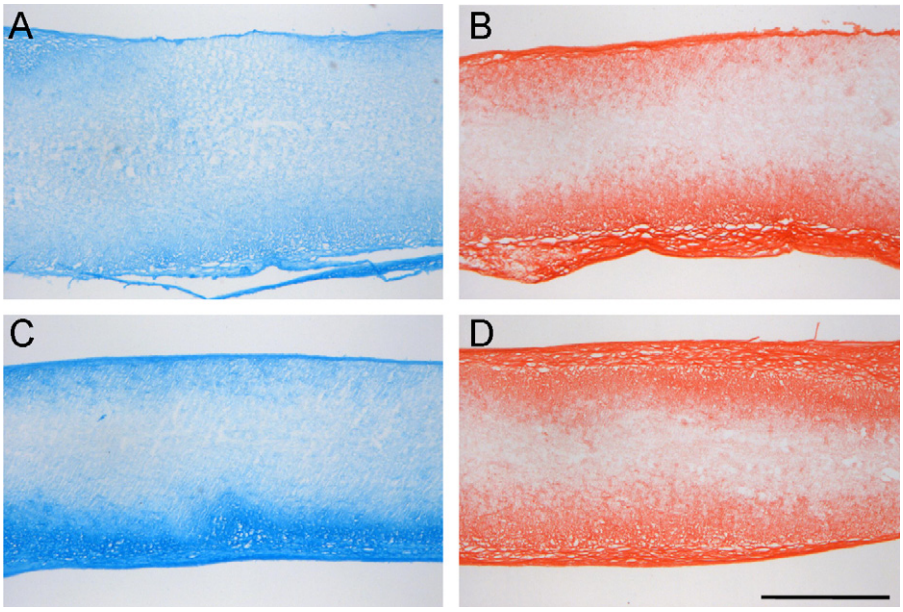

Fig. 6. Histological staining of collagen and proteoglycan (PG) deposition over the cross sections of cell-laden AL constructs on day 70. MFC- (A, B) and MSC- (C, D) laden AL nanofibrous stained with Alcian Blue (A, C) for PGs and Picrosirius Red (B, D) for collagens. PG deposition is observed throughout the scaffold, while collagen is restricted to the outer two-thirds. Scale bar: 500 μm.

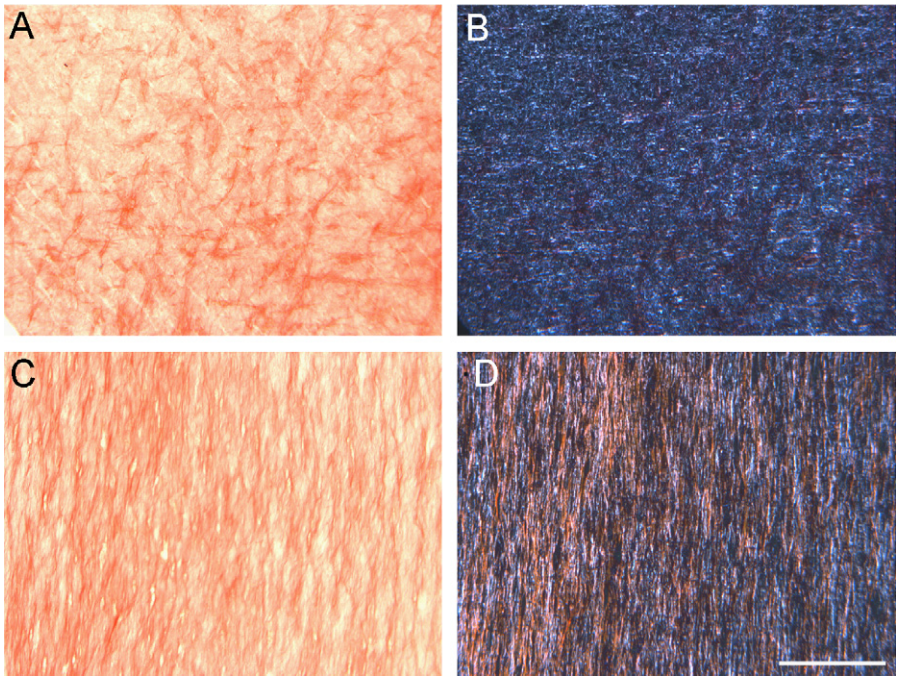

Fig. 7. Scaffold architecture influences the organization of forming neo-tissue with long-term culture. Bright-field (A, C) and polarized light (B, D) microscopy images of *en face* sections of NA (A, B) and AL (C, D) scaffolds seeded with MSCs on day 70. Sections were taken ~200 μm deep to the scaffold surface and stained with Picrosirius Red (PSR) to enhance birefringence of collagen stained areas (orange). Scale bar: 200 μm.

~1/3rd [31] that of the native tissue measured in the fiber direction. One explanation for this finding may be tied to development. Similar to such tissues as the annulus fibrosus of the intervertebral disk [50], AL meniscus cells arise first, prior to organized matrix deposition [51]. At this stage of development, if mechanical forces resulting from *in utero* muscle contraction are abrogated, the meniscus fails to mature and ultimately regresses [52]. Conversely, with continued normal motion, and more strikingly with load-bearing use, initial cellular organization presages a

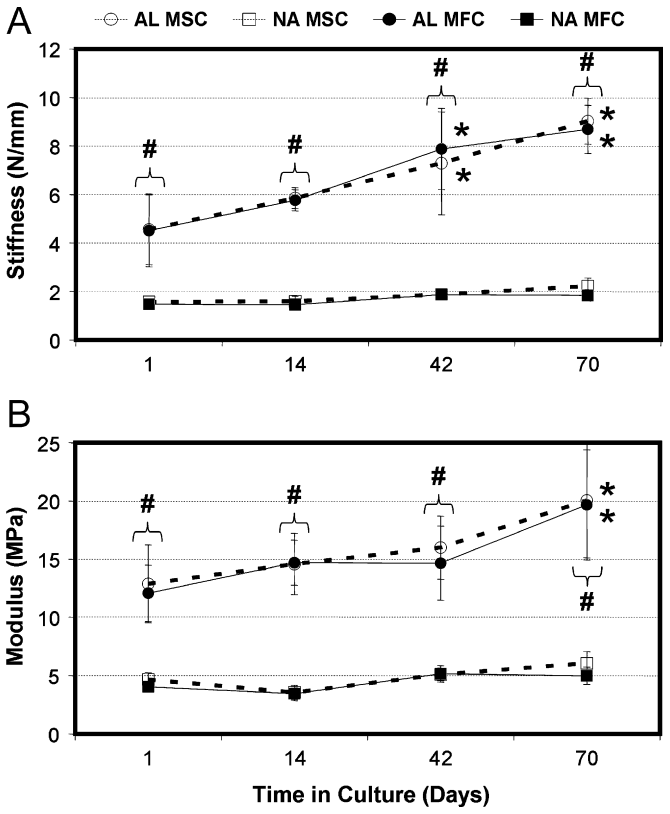

Fig. 8. Time-dependent changes mechanical properties of cell-laden constructs are dependent on starting scaffold architecture but not cell type. Tensile properties (stiffness: A; modulus: B) of MFC- and MSC-laden AL and NA nanofibrous scaffolds with time in culture. *Indicates $p<0.001$ vs. day 1 within group; #Indicates $p<0.001$ vs. NA within same cell type at same time point; $n=5$ per group per time point.

rapid and robust accumulation of dense fiber-reinforced ECM [51]. In this study, matured cell-seeded AL scaffolds possess the appropriate cell and matrix organization, but, like the developing native tissue, may require additional signals such as mechanical preconditioning to achieve properties comparable to the functionally differentiated adult load-bearing tissue.

A second limitation found in this study was the long time course required for mechanical properties to emerge. This slow accumulation in properties may be related to the rate at which cells colonize the scaffold interior. In this study, full colonization of ~1 mm thick scaffolds was achieved, but only between the 6- and 10-week culture time points (Fig. 5). Further, while cells colonized the entirety of the scaffold, their distribution and that of the forming matrix remained biased towards the outer periphery (Fig. 6). Similar findings have been noted in nanofibrous meshes of various compositions implanted in a rat model [53]. A number of strategies have been proposed to address this issue, including electrospraying cells directly into the forming nanofibrous scaffold during deposition [54]. Alternatively, design criteria may be imposed on polymer composition such that scaffold degradation is tuned to promote cellular colonization.

5. Conclusions

The results of this study demonstrate that AL nanofibrous scaffolds serve as a micro-pattern for directed tissue growth and that, when seeded with either MFCs or MSCs, produce constructs with improved mechanical properties compared to NA scaffolds. Importantly, these improvements were dependent on the organization of the forming neo-tissue, and not on its overall content. Furthermore, we showed that MSCs serve as a viable alternative, colonizing and forming ECM and mechanical properties on par with that formed by native MFCs. While properties improve substantially on AL scaffolds, these studies highlight the need for further optimization to achieve native tissue properties. Additional considerations, such as the inclusion of radial tie fibers and recapitulation of the anatomic wedge-shaped form, may also be important for improving construct integrity and *in vivo* application. If successful, these scaffolds will find wide application in the repair of meniscal defects, a prevalent and otherwise untreatable orthopedic condition. Further, these AL nanofibrous scaffolds may in general offer a ready solution to the challenge of tissue engineering other dense fibrous tissues of the musculoskeletal system whose mechanical function is critical to locomotion but whose endogenous repair is limited.

Acknowledgements

This work was funded by the Penn Center for Musculoskeletal Disorders (NIH AR050950). The authors gratefully acknowledge Nandan Nerurkar for his assistance with construction of the electrospinning device, and Ashwin Nathan, Robert Metter, and Andrea Tan for help with sample analysis. The authors also acknowledge Dr. Wan-Ju Li and Dr. Rocky S. Tuan (Cartilage Biology and Orthopaedics Branch, NIAMS, NIH, Bethesda, MD) for their seminal contributions to this work.

References

[1] Messner K, Gao J. The menisci of the knee joint. Anatomical and functional characteristics, and a rationale for clinical treatment. J Anat 1998;193(Pt 2):161–78.
[2] Greis PE, Bardana DD, Holmstrom MC, Burks RT. Meniscal injury: I. Basic science and evaluation. J Am Acad Orthop Surg 2002;10:168–76.
[3] Seedhom BB. Loadbearing function of the menisci. Physiotherapy 1976;62:223.
[4] Ahmed AM, Burke DL. In-vitro measurement of static pressure distribution in synovial joints—Part I: tibial surface of the knee. J Biomech Eng 1983;105:216–25.
[5] Shrive NG, O'Connor JJ, Goodfellow JW. Load-bearing in the knee joint. Clin Orthop 1978:279–87.
[6] Setton LA, Guilak F, Hsu EW, Vail TP. Biomechanical factors in tissue engineered meniscal repair. Clin Orthop 1999:S254–72.
[7] Fithian DC, Kelly MA, Mow VC. Material properties and structure–function relationships in the menisci. Clin Orthop 1990: 19–31.

[8] Petersen W, Tillmann B. Collagenous fibril texture of the human knee joint menisci. Anat Embryol (Berlin) 1998;197:317–24.
[9] Proctor CS, Schmidt MB, Whipple RR, Kelly MA, Mow VC. Material properties of the normal medial bovine meniscus. J Orthop Res 1989;7:771–82.
[10] McDevitt CA, Webber RJ. The ultrastructure and biochemistry of meniscal cartilage. Clin Orthop Relat Res 1990:8–18.
[11] Eyre DR, Wu JJ. Collagen of fibrocartilage: a distinctive molecular phenotype in bovine meniscus. FEBS Lett 1983;158:265–70.
[12] Adams ME, Hukins DWL. The extracellular matrix of the meniscus. In: Mow VC, Arnoczky SP, Jackson DW, editors. Knee meniscus: basic and clinical foundations. New York: Raven Press Ltd.; 1992. p. 15–28.
[13] O'Connor BL. The histological structure of dog knee menisci with comments on its possible significance. Am J Anat 1976;147: 407–17.
[14] Benjamin M, Ralphs JR. Biology of fibrocartilage cells. Int Rev Cytol 2004;233:1–45.
[15] MacAusland WR. Derangements of the semilunar cartilages. Ann Surg 1931;93:649–82.
[16] Cravener EK, MacElroy DG. Injuries of the internal semilunar cartilage. JAMA 1941;117:1695–700.
[17] Peretti GM, Gill TJ, Xu JW, Randolph MA, Morse KR, Zaleske DJ. Cell-based therapy for meniscal repair: a large animal study. Am J Sports Med 2004;32:146–58.
[18] Izuta Y, Ochi M, Adachi N, Deie M, Yamasaki T, Shinomiya R. Meniscal repair using bone marrow-derived mesenchymal stem cells: experimental study using green fluorescent protein transgenic rats. Knee 2005;12:217–23.
[19] Port J, Jackson DW, Lee TQ, Simon TM. Meniscal repair supplemented with exogenous fibrin clot and autogenous cultured marrow cells in the goat model. Am J Sports Med 1996;24:547–55.
[20] Buma P, Ramrattan NN, van Tienen TG, Veth RP. Tissue engineering of the meniscus. Biomaterials 2004;25:1523–32.
[21] Stone KR, Rodkey WG, Webber RJ, McKinney LA, Steadman XR. Development of a prosthetic meniscal replacement. In: Mow VC, Arnoczky SP, Jackson DW, editors. Knee meniscus: basic and clinical foundations. New York: Raven Press Ltd.; 1992. p. 165–73.
[22] Cook JL, Fox DB, Malaviya P, Tomlinson JL, Kuroki K, Cook CR, et al. Long-term outcome for large meniscal defects treated with small intestinal submucosa in a dog model. Am J Sports Med 2006;34: 32–42.
[23] Reneker DH, Chun I. Nanometre diameter fibres of polymer, produced by electrospinning. Nanotechnology 1996;7:216–23.
[24] Deitzel JM, Kleinmeyer J, Harris D, Beck Tan NC. The effect of processing variables on the morphology of electrospun nanofibers and textiles. Polymer 2001;42:261–72.
[25] Courtney T, Sacks MS, Stankus J, Guan J, Wagner WR. Design and analysis of tissue engineering scaffolds that mimic soft tissue mechanical anisotropy. Biomaterials 2006;27:3631–8.
[26] Matthews JA, Wnek GE, Simpson DG, Bowlin GL. Electrospinning of collagen nanofibers. Biomacromolecules 2002;3:232–8.
[27] Li WJ, Cooper Jr JA, Mauck RL, Tuan RS. Fabrication and characterization of six electrospun poly(alpha-hydroxy ester)-based fibrous scaffolds for tissue engineering applications. Acta Biomater 2006;2:377–85.
[28] Li WJ, Mauck RL, Tuan RS. Electrospun nanofibrous scaffolds: production, characterization, and applications for tissue engineering and drug delivery. J Biomed Nanotech 2005;1:259–75.
[29] Li M, Mondrinos MJ, Gandhi MR, Ko FK, Weiss AS, Lelkes PI. Electrospun protein fibers as matrices for tissue engineering. Biomaterials 2005;26:5999–6008.
[30] Li WJ, Mauck RL, Cooper JA, Yuan X, Tuan RS. Engineering controllable anisotropy in electrospun biodegradable nanofibrous scaffolds for musculoskeletal tissue engineering. J Biomech 2006.
[31] Baker BM, Sheth NP, Mauck RL. Maturation of MFC- and MSC-laden nanofibrous scaffolds for meniscus tissue engineering. In: Proceedings of BIO2006 summer bioengineering conference, Paper #157580, 2006.
[32] Li WJ, Tuli R, Okafor C, Derfoul A, Danielson KG, Hall DJ, et al. A three-dimensional nanofibrous scaffold for cartilage tissue engineering using human mesenchymal stem cells. Biomaterials 2005;26: 599–609.
[33] Theron A, Zussman E, Yarin AL. Electrostatic field-assisted alignment of electrospun nanofibres. Nanotechnology 2001;12: 384–90.
[34] Boland ED, Wnek GE, Simpson DG, Pawlowski KJ, Bowlin GL. Tailoring tissue engineering scaffolds using electrostatic processing techniques: a study of poly(glycolic acid) electrospinning. J Macromol Sci 2001;A38:1231–43.
[35] Ayres C, Bowlin GL, Henderson SC, Taylor L, Shultz J, Alexander J, et al. Modulation of anisotropy in electrospun tissue-engineering scaffolds: analysis of fiber alignment by the fast Fourier transform. Biomaterials 2006;27:5524–34.
[36] Nerurkar NL, Baker BM, Chen CY, Elliott DM, Mauck RL. Engineering of fiber-reinforced tissue with anisotropic biodegradable nanofibrous scaffolds. In: Transactions of the 28th Ann IEEE-EMBS meeting, 2006. p. 787–90.
[37] Li WJ, Mauck RL, Cooper Jr JA, Yuan X, Tuan RS. Engineering controllable anisotropy in electrospun biodegradable nanofibrous scaffolds for musculoskeletal tissue engineering. J Biomech 2006; in press.
[38] Mauck RL, Martinez-Diaz GJ, Yuan X, Tuan RS. Regional variation in meniscal fibrochondrocyte multi-lineage differentiation potential: implications for meniscal repair. Anat Rec 2006; in press.
[39] Mauck RL, Yuan X, Tuan RS. Chondrogenic differentiation and functional maturation of bovine mesenchymal stem cells in long-term agarose culture. Osteoarthritis Cartil 2006;14:179–89.
[40] Venugopal J, Ma LL, Yong T, Ramakrishna S. In vitro study of smooth muscle cells on polycaprolactone and collagen nanofibrous matrices. Cell Biol Int 2005;29:861–7.
[41] Farndale RW, Buttle DJ, Barrett AJ. Improved quantitation and discrimination of sulphated glycosaminoglycans by use of dimethylmethylene blue. Biochim Biophys Acta 1986;883: 173–7.
[42] Stegemann H, Stalder K. Determination of hydroxyproline. Clin Chim Acta 1967;18:267–73.
[43] Mrksich M, Dike LE, Tien J, Ingber DE, Whitesides GM. Using microcontact printing to pattern the attachment of mammalian cells to self-assembled monolayers of alkanethiolates on transparent films of gold and silver. Exp Cell Res 1997;235:305–13.
[44] Wheeler BC, Corey JM, Brewer GJ, Branch DW. Microcontact printing for precise control of nerve cell growth in culture. J Biomech Eng 1999;121:73–8.
[45] Wang JH, Jia F, Gilbert TW, Woo SL. Cell orientation determines the alignment of cell-produced collagenous matrix. J Biomech 2003;36:97–102.
[46] Lee CH, Shin HJ, Cho IH, Kang YM, Kim IA, Park KD, et al. Nanofiber alignment and direction of mechanical strain affect the ECM production of human ACL fibroblast. Biomaterials 2005;26: 1261–70.
[47] Pittenger MF, Mackay AM, Beck SC, Jaiswal RK, Douglas R, Mosca JD, et al. Multilineage potential of adult human mesenchymal stem cells. Science 1999;284:143–7.
[48] Barry F, Boynton RE, Liu B, Murphy JM. Chondrogenic differentiation of mesenchymal stem cells from bone marrow: differentiation-dependent gene expression of matrix components. Exp Cell Res 2001;268:189–200.
[49] Upton ML, Chen J, Setton LA. Region-specific constitutive gene expression in the adult porcine meniscus. J Orthop Res 2006;24: 1562–70.
[50] Hayes AJ, Benjamin M, Ralphs JR. Role of actin stress fibres in the development of the intervertebral disc: cytoskeletal control of extracellular matrix assembly. Dev Dyn 1999;215:179–89.

[51] Clark CR, Ogden JA. Development of the menisci of the human knee joint. Morphological changes and their potential role in childhood meniscal injury. J Bone Joint Surg Am 1983;65:538–47.
[52] Mikic B, Johnson TL, Chhabra AB, Schalet BJ, Wong M, Hunziker EB. Differential effects of embryonic immobilization on the development of fibrocartilaginous skeletal elements. J Rehabil Res Dev 2000;37:127–33.
[53] Telemeco TA, Ayres C, Bowlin GL, Wnek GE, Boland ED, Cohen N, et al. Regulation of cellular infiltration into tissue engineering scaffolds composed of submicron diameter fibrils produced by electrospinning. Acta Biomater 2005;1:377–85.
[54] Stankus JJ, Guan J, Fujimoto K, Wagner WR. Microintegrating smooth muscle cells into a biodegradable, elastomeric fiber matrix. Biomaterials 2006;27:735–44.